UNIVERSITY OF LEEDS

This is a repository copy of *New strategies for colloidal-quantum-dot-based intermediate-band solar cells*.

White Rose Research Online URL for this paper:
http://eprints.whiterose.ac.uk/154212/

Version: Supplemental Material

Article:

Califano, M orcid.org/0000-0003-3199-3896, Skibinsky-Gitlin, ES, Gómez-Campos, FM et al. (1 more author) (2019) New strategies for colloidal-quantum-dot-based intermediate-band solar cells. The Journal of Chemical Physics, 151 (15). 154101. ISSN 0021-9606

https://doi.org/10.1063/1.5121360

© 2019 Author(s). This is an author produced version of an article published in Journal of Chemical Physics. Uploaded in accordance with the publisher's self-archiving policy.

Reuse
Items deposited in White Rose Research Online are protected by copyright, with all rights reserved unless indicated otherwise. They may be downloaded and/or printed for private study, or other acts as permitted by national copyright laws. The publisher or other rights holders may allow further reproduction and re-use of the full text version. This is indicated by the licence information on the White Rose Research Online record for the item.

Takedown
If you consider content in White Rose Research Online to be in breach of UK law, please notify us by emailing eprints@whiterose.ac.uk including the URL of the record and the reason for the withdrawal request.

White Rose university consortium
Universities of Leeds, Sheffield & York

eprints@whiterose.ac.uk
https://eprints.whiterose.ac.uk/

Supporting Information: New Strategies for Colloidal-Quantum-Dot-Based Intermediate-Band Solar Cells

Marco Califano,[*,†] Erik S. Skibinsky-Gitlin,[‡] Francisco M. Gómez-Campos,[‡,¶] and Salvador Rodríguez-Bolívar[‡,¶]

Pollard Institute, School of Electronic & Electrical Engineering, and Bragg Centre for Materials Research, University of Leeds, Leeds LS2 9JT, United Kingdom, Departamento de Electrónica y Tecnología de Computadores, Facultad de Ciencias, Universidad de Granada, 18071 Granada, Spain, and CITIC-UGR, C/ Periodista Rafael Gómez Montero, n 2, Granada, Spain

E-mail: *m.califano@leeds.ac.uk

[*]To whom correspondence should be addressed

[†]Pollard Institute, School of Electronic & Electrical Engineering, and Bragg Centre for Materials Research, University of Leeds, Leeds LS2 9JT, United Kingdom

[‡]Departamento de Electrónica y Tecnología de Computadores, Facultad de Ciencias, Universidad de Granada, 18071 Granada, Spain

[¶]CITIC-UGR

Theoretical method

We consider perfectly crystalline, identical, nearly-spherical zincblende InAs nanocrystals, arranged in oriented and perfectly ordered 2D square arrays, with a minimum inter-dot separation corresponding to one bond length (0.26 nm for InAs). These seemingly strongly idealised systems are indeed realistically achievable experimentally, thanks to recent advances in synthetic methods[1–3] and to the increased ability to engineer the length of the nanocrystals' capping groups,[4–8] which have led to the creation of quantum dot superlattices with long-range order on the micrometre scale.[2,3] The electronic states of such periodic systems are obtained within the tight-binding approach,[9] by expanding the superlattice wave functions in a basis of single quantum dot conduction band eigenstates $\phi_n(\vec{r})$ obtained within the atomistic semiempirical pseudopotential framework[10] (where electron surface trap states are modelled according to the procedure detailed in Ref. 11), and can be expressed in terms of Bloch functions as

$$u_{n,\vec{q}}(\vec{r})\, e^{i\vec{q}\cdot\vec{r}} = \left[\sum_m \sum_{\vec{R}_n} b_m e^{i\vec{q}\cdot\left(\vec{R}_n-\vec{r}\right)} \phi_m\left(\vec{r}-\vec{R}_n\right)\right] e^{i\vec{q}\cdot\vec{r}}.$$

where b_m are the coefficients of the expansion (we use up to 9 wave functions for each - conduction and valence - band of the isolated quantum dot), $\vec{R}_n$ are the superlattice vectors and $\vec{q}$ is a vector of the superlattice reciprocal space.

The absorption coefficient is calculated within the electric dipole approximation using Fermi's Golden Rule, as

$$\alpha(\hbar\omega) = \frac{2\pi e^2}{Q_{st} v_{unitcell} n_r c \epsilon_0 \Delta E} \sum_f \sum_i \frac{\omega}{K_i K_f} \left|\hat{e}\cdot\langle u_f|\vec{r}|u_i\rangle_{unitcell}\right|^2 \left(f(E_i)-f(E_f)\right)$$

where e is the electron charge, Q_{st} is the number of vectors of the reciprocal space for which the Schrödinger equation is solved (a 501×501 grid discretisation is used here to

sample the Brillouin zone), $v_{unitcell}$ is the volume of the superlattice unit cell, n_r is the refractive index of the material, c is the speed of light in vacuum, ϵ_0 is the vacuum dielectric constant, ΔE is the interval width within which energy is conserved,[12] ω is the angular frequency of the photon involved in the absorption process, K_n is related to the normalisation constant $1/\sqrt{K_{\vec{q}} N_s}$ (where N_s is the number of quantum dots in the superlattice), $\hat{e}$ is the potential vector polarisation, u_f and u_i are the Bloch functions of the superlattice wave function for the final (f) and initial (i) states, and $f(E)$ is Fermi-Dirac's statistics.

Atomistic modelling of single NCs

In our atomistic approach the NC is built with bulk-like structure, starting from its constituent atoms, from its centre outwards up to the desired radius. This procedure yields surface atoms with unsaturated bonds. Atoms with only one (saturated) bond are removed, leaving on the surface only atoms with one or two missing bonds. These surface dangling bonds are passivated by pseudo-hydrogenic, short-range potentials with Gaussian form, positioned along the line connecting the missing bonding atom and the passivated atom, at a distance $0 < d < D_{\text{bulk}}$ (where D_{bulk} is the bulk bond length) from the centre of the latter.[13,14] This method is not meant to simulate specific ligands, but represents rather a generic passivation that aims at removing states in the gap. Electron surface trap states are modelled according to the procedure detailed in Ref. 11. For each dot size considered, among the different traps we created (in terms of both spatial position on the surface and energetic position - i.e., depth - in the gap), we selected those with an energy separation from the CBM close to the optimum separation (~ 0.9 eV) suggested by Luque and Marti[15] for maximum solar conversion efficiency.

As it is the case with any non-self-consistent (i.e., non-DFT) method,[16] the structure is not relaxed nor the surface is allowed to reconstruct, since with realistic experimental sizes, this energy minimisation step is prohibitively expensive computationally and

cannot be performed self-consistently.

3D Charge densities of isolated NCs

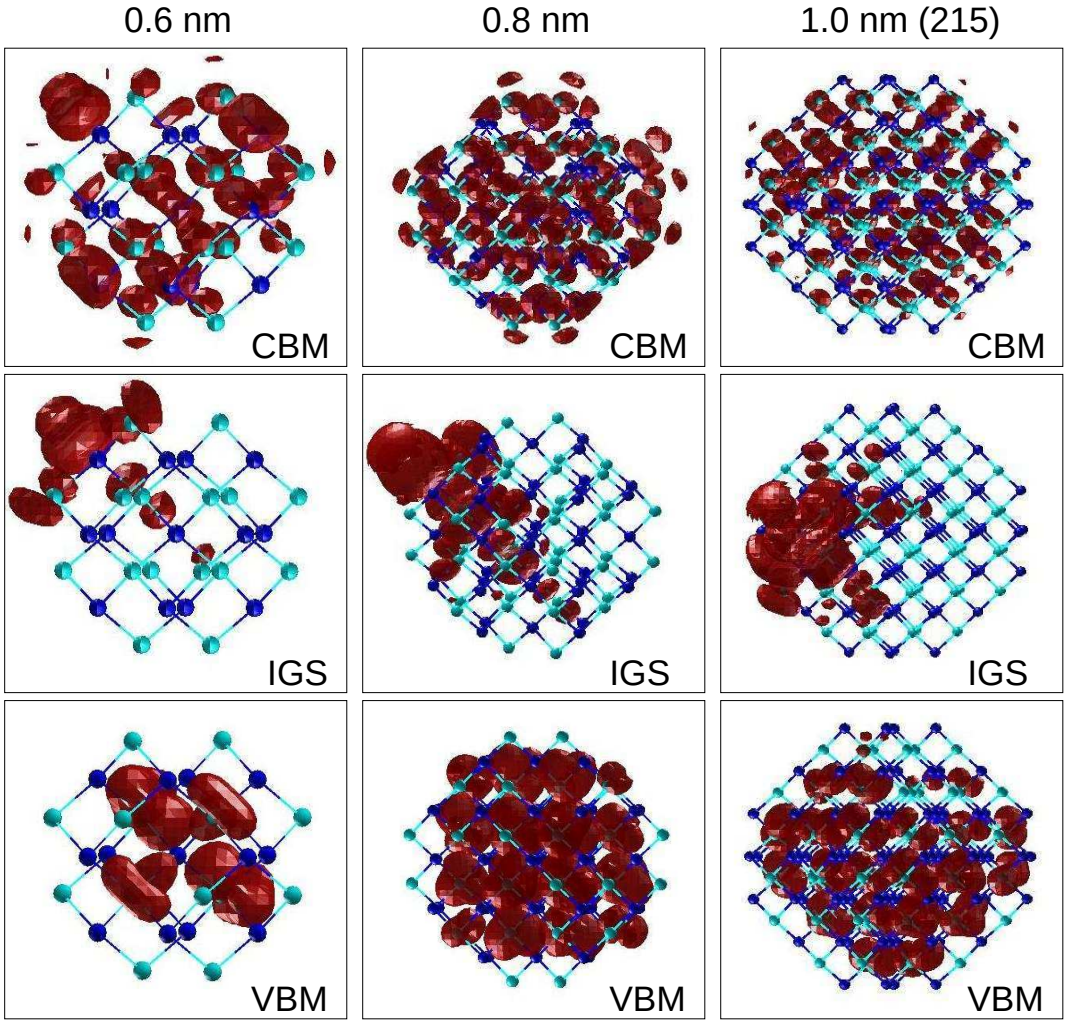

Figure S 1: Calculated 3D charge density (dark red) of CBM, IGS and VBM in isolated InAs CQDs with $R = 0.6$, 0.8, and 1.0 nm. The blue and cyan spheres represent In and As atoms, respectively.

Optical spectra of isolated NCs

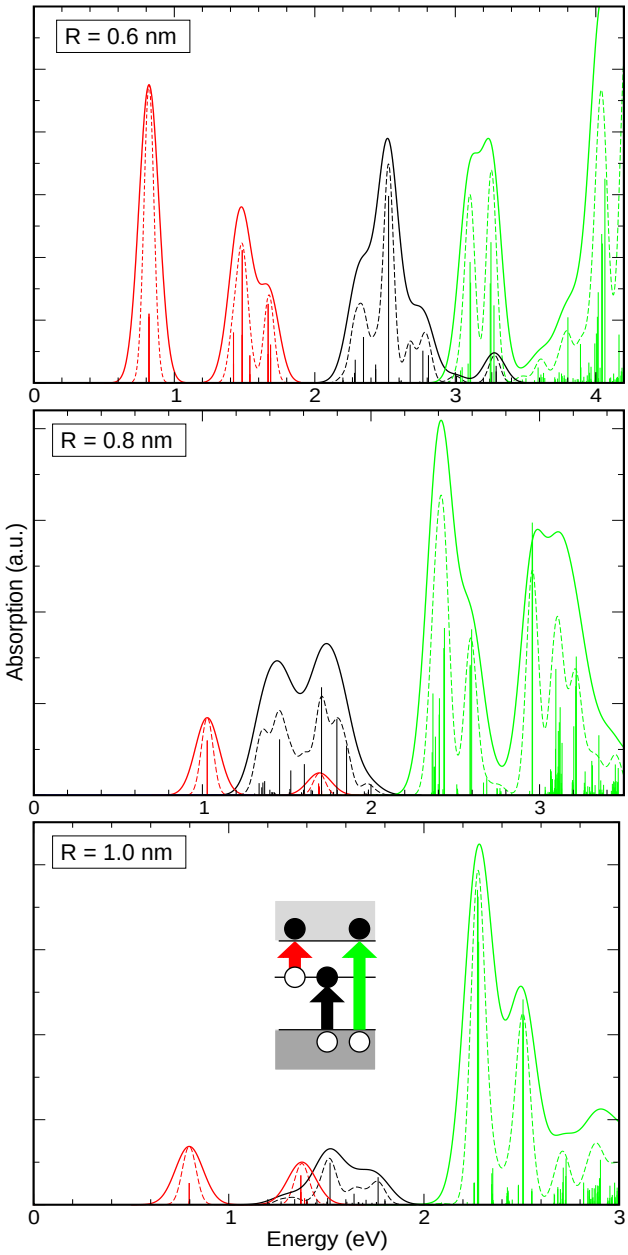

Figure S 2: Absorption spectra of isolated InAs CQDs with $R = 0.6$, 0.8, and 1.0 nm. The vertical lines represent the probability for each transition. The colour of the different contributions to the spectra reflects the different transitions they refer to, according to the inset. Experimental broadening is reproduced here using Gaussian broadenings of 50 meV (dashed lines) and 100 meV (solid lines).

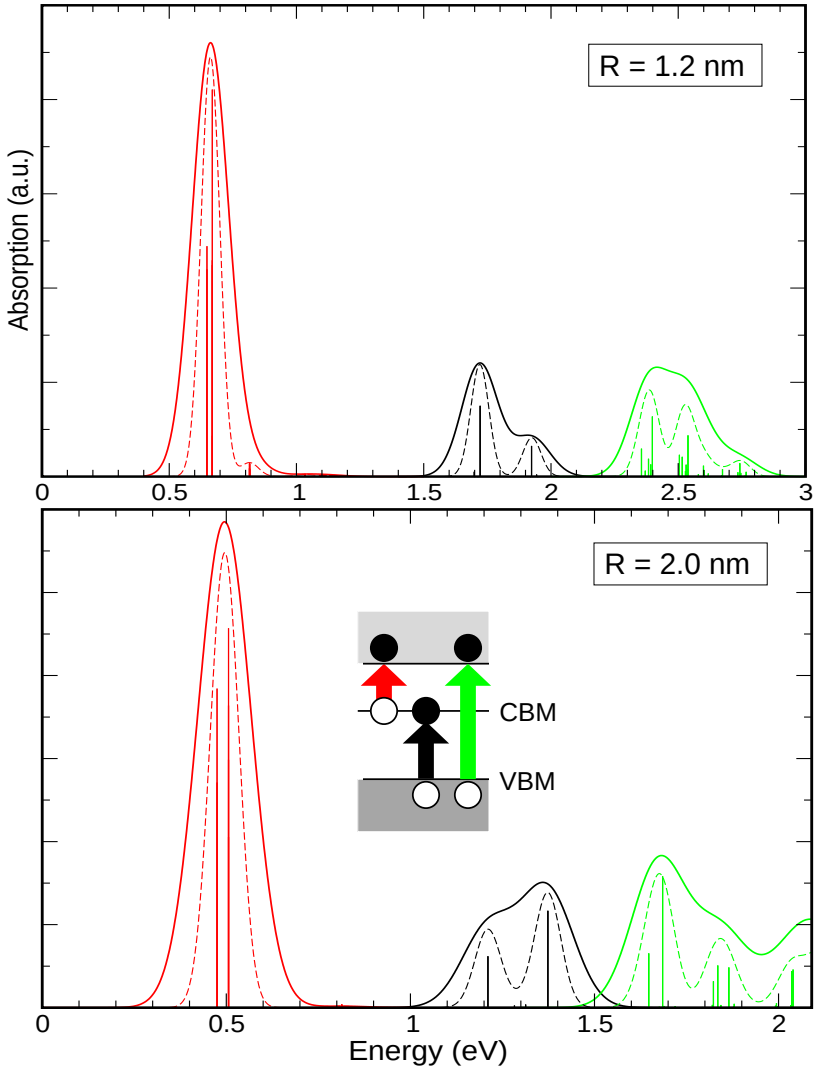

Figure S 3: Absorption spectra of isolated InAs CQDs with $R = 1.2$ and 2.0 nm. The vertical lines represent the probability for each transition. The colour of the different contribution to the spectra reflects the different transitions they refer to, according to the inset. Experimental broadening is reproduced here using Gaussian broadenings of 50 meV (dashed lines) and 100 meV (solid lines).

3D band structure of a film of InAs NCs with $R = 0.6$ nm

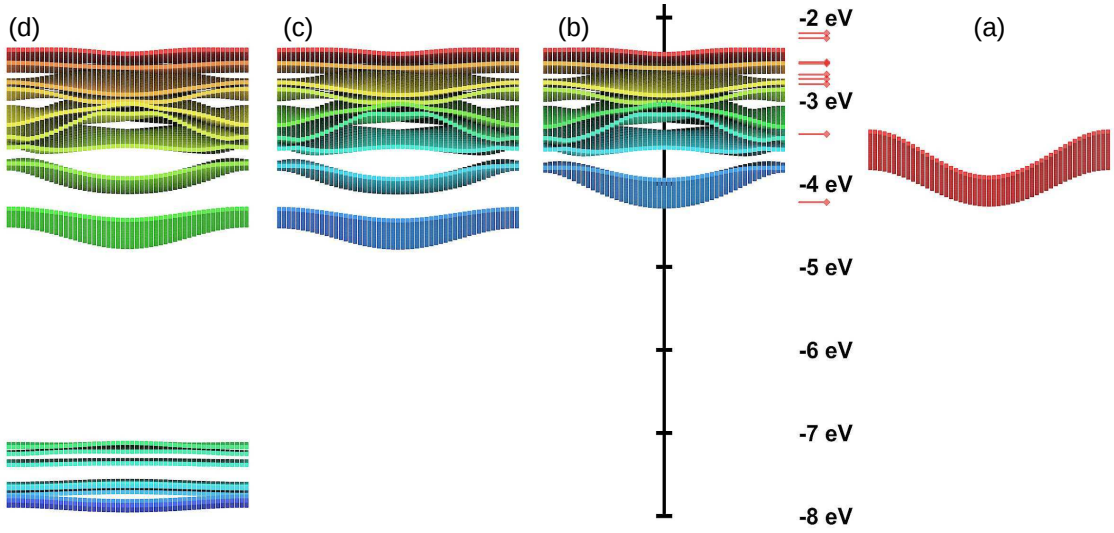

Figure S 4: Evolution of the CBM miniband position and width in a film of InAs CQDs with $R = 0.6$ nm, obtained considering coupling with the following states in neighbouring NCs: (a) only the CBM, (b) CBM plus higher CB states, (c) all CB states (including the IGS), (d) all states (including the VB). It is clear that both energy position and width depend on the coupling with higher CB states (b) but are not influenced by the presence of either VB states (d) or IGS (c). The energy levels of the isolated dot are shown as horizontal red lines. The energies are referred to the vacuum level.

Absorption edge peak energies in isolated NCs and quantum dot films

Table S 1: Band edge peak transition energies E_{IC}, E_{VI} and E_g, for the IB→CBM, VBM→IB, and VBM→CBM transitions, respectively, used for estimating the IBSC limiting efficiencies at 1 sun (AM1.5G) and 100 suns (AM1.5D), according to Bremner, Levy and Honsberg[17] and to Krishna and Krich,[18] for InAs NCs both isolated and in a close-packed film, reported in Table I, main text. For $R \leq 1.0$ nm the IB is the IGS, whereas in the case of $R = 1.2$ nm and $R = 2.0$ nm the CBM is considered as the IB, therefore the "real" band gap energies are E_{VI}, whereas the values for E_g reported in the last two rows of the table are relative to the VBM→CBM+1 transition.

	Isolated			Film		
R[nm]	E_{IC}[eV]	E_{VI}[eV]	E_g[eV]	E_{IC}[eV]	E_{VI}[eV]	E_g[eV]
	IB=IGS					
0.6	0.825	2.291	3.108	0.62	2.156	2.385
0.8	1.032	1.341	2.370	0.56	1.021	1.514
1.0	0.800	1.520	2.258	0.98	1.467	2.400
	IB=CBM					
1.2	0.651	1.725	2.358	0.906	1.545	1.788
2.0	0.480	1.215	1.650	0.480	1.258	1.672

3D oscillator strength in a film of InAs NCs with $R = 1.2$ nm

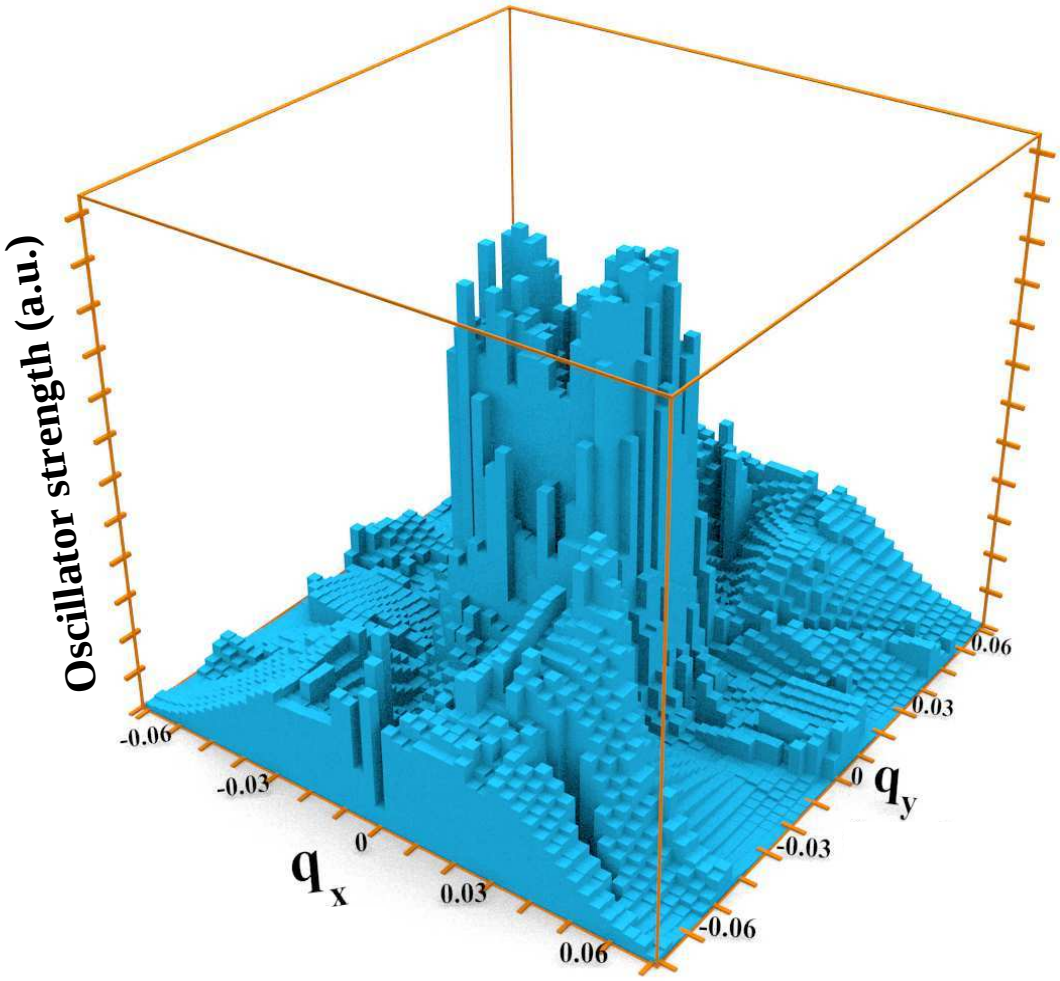

Figure S 5: 3D representation of the oscillator strength vs $\vec{q}$ for transitions originating from M_1 to M_2 calculated for films of InAs CQDs with $R = 1.2$ nm where the interdot separation is one bond length

Evolution of the band structure with dot-to-dot separation in a film of InAs NCs with $R = 1.2$ nm

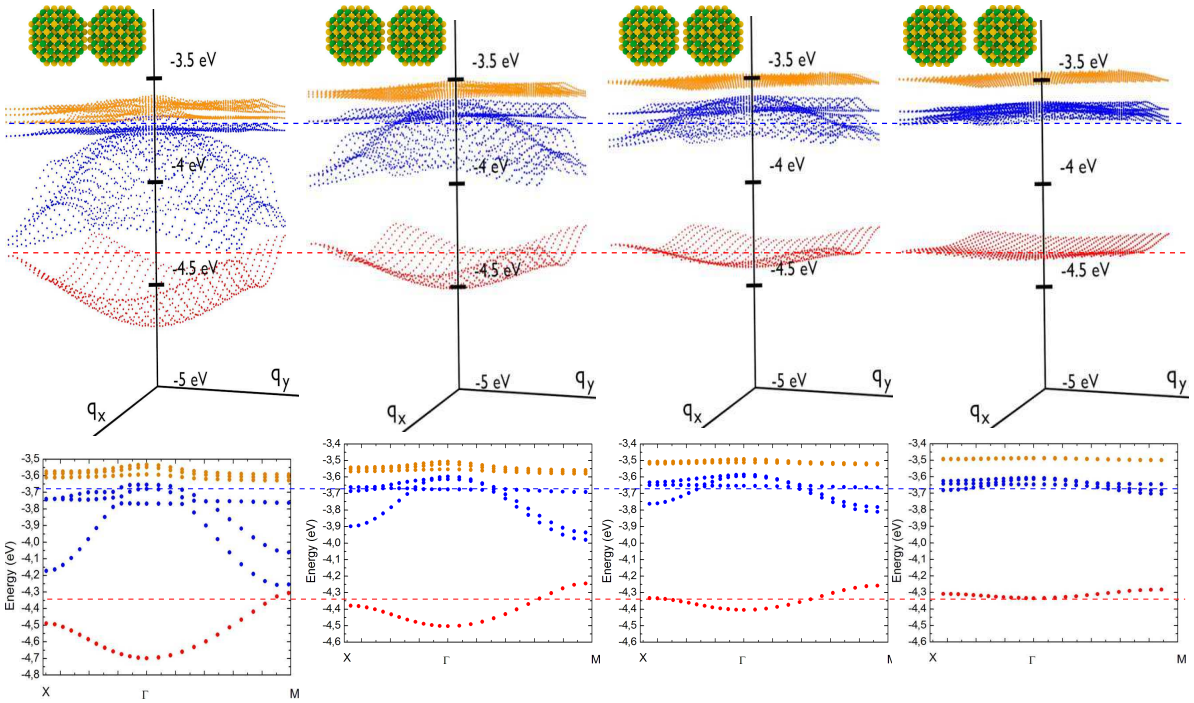

Figure S 6: Conduction band structure calculated for films of InAs CQDs with $R = 1.2$ nm for different values of the interdot separation, ranging from one bond length (left panel) to two bond lengths (right panel). The dashed lines mark the position of the CBM (red lines) and CBM+1 (blue lines) in isolated dots. The inset at the top indicate the interdot separation. Bottom panels are 2D representation of the band structure.

References

(1) Murray, C. B., Kagan, C. R. and Bawendi, M. G. Synthesis and Characterization of Monodisperse Nanocrystals and Close-Packed Nanocrystal Assemblies *Annu. Rev. Mater. Sci.* **2000**, *30*, 545-610.

(2) Weidman, M. C.; Beck, M. E.; Hoffman, R. S.; Prins, F.; Tisdale, W. A. Monodisperse, Air-Stable PbS Nanocrystals via Precursor Stoichiometry Control. *ACS Nano* **2014**, *8*, 6363-6371.

(3) Maulu, A.; Rodríguez Cantó, P. J.; Navarro Arenas, J.; Abargues, R.; Sanchez-Royo, J. F.; García Calzada, R.; Martínez-Pastor, J. P. Strongly-Coupled PbS QD Solids by Doctor Blading for IR Photodetection *RSC Adv.* **2016**, *6*, 80201-80212.

(4) Choi, J.-H.; Fafarman, A. T.; Oh, S. J.; Ko, D.-K.; Kim, D. K.; Diroll, B. T.; Muramoto, S.; Gillen, J. G.; Murray, C. B.; Kagan, C. R. Bandlike Transport in Strongly Coupled and Doped Quantum Dot Solids: A Route to High-Performance Thin-Film Electronics. *Nano Lett.* **2012**, *12*, 2631-2638.

(5) Baumgardner, W. J.; Whitham, K.; Hanrath, T. Confined-but-Connected Quantum Solids via Controlled Ligand Displacement *Nano Lett.* **2013**, *13*, 3225-3231.

(6) Cho, K.-S.; Talapin, D. V.; W. Gaschler, W.; Murray, C. B. *J. Am. Chem. Soc.* **2005**, *127*, 7140-7147.

(7) Schliehe, C.; Juarez, B. H.; Pelletier, M.; Jander, S.; Greshnykh, D.; Nagel, M.; Meyer, A.; Foerster, S.; Kornowski, A.; Klinke, C.; Weller, H. *Science* **2010**, *329*, 550-553.

(8) Evers, W. H.; Goris, B.; Bals, S.; Casavola, M.; de Graaf, J.; van Roij, R.; Dijkstra, M.; and Vanmaekelbergh, D. *Nano Lett*. **2013**, *13*, 2317-2323.

(9) Ashcroft, N. W.; Mermin, N. *Solid State Physics*, Holt Rinehart and Winston, New York, London, 1976.

(10) Gómez-Campos, F. M.; Rodríguez-Bolívar, S.; Califano, M. High-Mobility Toolkit for Quantum Dot Films. *ACS Photonics* **2016**, *3*, 2059-2067.

(11) Zhu, H.; Yang, Y.; Hyeon-Deuk, K.; Califano, M.; Song, N.; Wang, Y.; Zhang, W.; Prezhdo, O. V.; Lian, T. Auger-Assisted Electron Transfer from Photoexcited Semiconductor Quantum Dots. *Nano Lett.* **2014**, *14*, 1263-1269.

(12) In order to simplify the calculations, Dirac's delta function is broadened here using a box function of width ΔE, instead of the conventional Gaussian or Lorentzian functions.

(13) Wang, L.-W.; Zunger, A. Pseudopotential Calculations of Nanoscale CdSe Quantum Dots. *Phys. Rev. B* **1996**, *53*, 9579-9582.

(14) Bester, G. Electronic Excitations in Nanostructures: An Empirical Pseudopotential Based Approach *J. Phys.: Condens. Matter* **2009**, *21*, 023202.

(15) Luque, A.; Marti, A. Increasing the Efficiency of Ideal Solar Cells by Photon Induced Transitions at Intermediate Levels *Phys. Rev. Lett.* **1997**, *78*, 5014.

(16) Delerue, C. From Semiconductor Nanocrystals to Artificial Solids with Dimensionality Below Two. *Phys. Chem. Chem. Phys.* **2014**, *16*, 25734-25740.

(17) Bremner, S. P.; Levy, M. Y.; Honsberg, C. B. Limiting Efficiency of an Intermediate Band Solar Cell under a Terrestrial Spectrum *Appl. Phys. Lett.* **2008**, *92*, 171110.

(18) Krishna, A.; Krich, J. J. Increasing Efficiency in Intermediate Band Solar Cells with Overlapping Absorptions *J. Opt.* **2016**, *18*, 074010-1–074010-7.